

City-Wide Low-Altitude Urban Air Mobility: A Scalable Global Path Planning Approach via Risk-Aware Multi-Scale Cell Decomposition

Josue N. Rivera¹, Dengfeng Sun², and Chen Lv¹

Abstract—The realization of Urban Air Mobility (UAM) necessitates scalable global path planning algorithms capable of ensuring safe navigation within complex urban environments. This paper proposes a multi-scale risk-aware cell decomposition method that efficiently partitions city-scale airspace into variable-granularity sectors, assigning each cell an analytically estimated risk value based on obstacle proximity and expected risk. Unlike uniform grid approaches or sampling-based methods, our approach dynamically balances resolution with computational speed by bounding cell risk via Mahalanobis distance projections, eliminating exhaustive field sampling. Comparative experiments against classical A*, Artificial Potential Fields (APF), and Informed RRT* across five diverse urban topologies demonstrate that our method generates safer paths with lower cumulative risk while reducing computation time by orders of magnitude. The proposed framework, *Larp Path Planner*, is open-sourced and supports any map provider via its modified GeoJSON internal representation, with experiments conducted using OpenStreetMap data to facilitate reproducible research in city-wide aerial navigation.

Keywords: Urban Air Mobility, path planning, cell decomposition, risk-aware navigation, OpenStreetMap

I. INTRODUCTION

The realization of Urban Air Mobility (UAM) promises a transformative shift in metropolitan transportation, envisioning a three-dimensional ecosystem for the efficient movement of passengers and goods [1], [2]. Within this domain, small Autonomous Aerial Vehicles (AAVs) for logistical operations such as aerial cargo delivery are anticipated to be among the earliest adopters [3]. However, AAV deployment in dense, low-altitude urban environments introduces profound safety and scalability challenges. Unlike high-altitude airspace, the urban canyon is cluttered with static obstacles, dynamic uncertainties, and stringent regulatory restrictions, necessitating navigation solutions that prioritize operational safety and risk minimization [4]–[6].

Global path planning remains a fundamental component of autonomous navigation. Existing literature categorizes planning strategies into sampling-based and node-based approaches [7], [8]. Sampling-based methods such as Informed-RRT* [9], [10] excel in high-dimensional spaces but incur high computational costs unsuitable for real-time city-scale planning. Node-based

approaches like A* provide optimality and speed but suffer from memory scalability issues on high-resolution uniform grids [11], [12]. Hierarchical decomposition structures (including quadtree and octree representations) reduce this combinatorial cost, yet existing implementations treat decomposition as a purely geometric operation, assigning no risk information to individual cells [8]. Artificial Potential Field (APF) methods offer reactive efficiency but are prone to local minima in complex obstacle configurations [13]–[15]. Recent learning-based planners have also been explored for UAV navigation, though they typically require environment-specific training and lack formal safety guarantees [16].

Recent research has pivoted toward cost-map-based planning, penalizing spatial regions based on obstacle proximity, population exposure, or ground impact risk [17], [18]. While effective, these methods share a common limitation: the underlying spatial representation remains a uniform discrete grid whose resolution must be set globally to guarantee safety in the narrowest passages, causing combinatorial explosion at city scale.

The core challenge is therefore finding safe paths at city scale in near-real-time, a combination no existing method fully achieves. This paper addresses this through a principled multi-scale cell decomposition in which each cell is assigned an analytically estimated risk value derived from a standardized urban risk field. Given any city’s map (loaded directly from OpenStreetMap or via GeoJSON), the framework automatically computes a hierarchical decomposition where every cell carries a conservative risk bound, computed via Mahalanobis distance projection without exhaustive field sampling. This risk-annotated representation is then used by a modified A* planner that penalizes high-risk cells, naturally steering routes through safer corridors. Adaptive granularity concentrates resolution near hazards and coarsens over open airspace, making the approach both distance-competitive and scalable. Prior hierarchical decomposition methods treat subdivision as a purely geometric operation with no risk information per cell [8]; cost-map approaches encode risk but over uniform grids that cause combinatorial explosion at city scale [17], [18]. To the authors’ knowledge, *Larp* is the first aerial framework to assign analytically bounded risk values to individual cells of an adaptive decomposition, combining the scalability of quadtree structures with the safety guarantees of risk-field-based routing for city-scale global path planning.

We introduce *Larp Path Planner* (Last-mile Autonomous Route Planning Path Planner), a domain-agnostic global path

This work was supported in part by the Ministry of Education (MOE), Singapore, under the Tier 2 Grant (MOE-T2EP50222-0002), and the NTUitive Gap Fund, Nanyang Technological University.

¹Josue N. Rivera and Chen Lv are with the School of Mechanical and Aerospace Engineering, Nanyang Technological University, Singapore {josue.rivera, lyu}@ntu.edu.sg

²Dengfeng Sun is with the School of Aeronautics and Astronautics, Purdue University, West Lafayette, IN 47907, USA dsun@purdue.edu

planning framework for restrictive routing within standardized “risk fields” [19], demonstrated here through aerial cargo transport scenarios. The remainder of this paper is organized as follows. Section II defines the standardized risk field. Section III presents the multi-scale decomposition and risk-aware graph search. Section IV reports comparative results across five urban environments. Section V concludes with directions for future work.

II. PRELIMINARIES

A. Risk Fields

In [19], an unmanned aerial traffic management (UTM) system was proposed for last-mile urban air mobility that restricts UAVs to operating altitude ranges, or channels. As part of the system, a standard was introduced for defining an urban risk/cost field based on the concept of repulsion potential fields to limit routes. Physical restrictions at or above the operating altitude range of UAVs and virtual restrictions are designated as areas of high potential that diminish away from the obstacles; a behavior dictated by the individual repulsion matrix.

The standardization facilitates a uniform approach to continuous risk field construction for UAM, enabling consistent replication and analysis across different urban settings. By leveraging the structured nature of the risk field, algorithms can be developed to navigate through complex environments utilizing a common standard, avoiding obstacles, and minimizing the risk of restriction violations. The field delineated herein is henceforth denoted as a ‘risk field’.

B. Standardized Field Units

Under the proposed standard, a risk field is comprised of multiple building blocks, each corresponding to a distinct type of restriction. Upon examining their definitions, a set of intrinsic properties emerges: a repulsion vector \bar{x} , a squared Mahalanobis distance $\tilde{d}^2(x)$, and a risk $\sigma(x)$. The repulsion vector \bar{x} encodes the direction and proximity from the restricted areas. The squared Mahalanobis distance $\tilde{d}^2(x)$ reflects the weighted proximity to a point x , modulated by the unit’s repulsion matrix A . Finally, the risk potential $\sigma(x)$ denotes the field’s influence at point x , effectively reflecting the risk for restriction violation.

The repulsion vectors of the fundamental units and collection of them are detailed in Table I. For full comparability with GeoJSON, an additional Polygon unit is included. Fig. 1 illustrates the repulsion vectors for an arbitrary set of obstacles with respect to an arbitrary point. The magnitude of each vector indicates proximity to the obstacle and the direction provides a guide towards moving away from it.

Definition 1 (Squared Distance to an Unit): A proxy to the squared distance to a risk field unit $d^2(x)$ is defined as:

$$d^2(x) = \bar{x}(x)^T \bar{x}(x),$$

where $\bar{x}(x)$ is the repulsion vector detailed in Table I and x is an evaluated point. For a collection of units, $d^2(x)$ is the smallest squared distance among all sub-units.

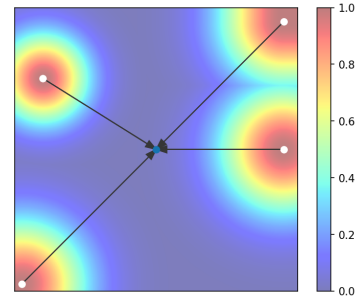


Fig. 1: Repulsion vectors encoding distance and direction from nearby obstacles to an evaluation point (blue dot).

Definition 2 (Squared Mahalanobis Distance to an Unit):

The squared Mahalanobis distance to a risk field unit $\tilde{d}^2(x)$ is defined as:

$$\tilde{d}^2(x) = \bar{x}(x)^T A^{-1} \bar{x}(x),$$

where $\bar{x}(x)$ is again the repulsion vector from Table I, A is the positive definite repulsion matrix of the unit, and x is an evaluated point. In the case of a collection of units, $\tilde{d}^2(x)$ is the minimum of the squared Mahalanobis distances with respect to its sub-units.

Definition 3 (Risk with Respect to an Unit): The risk with respect to a unit $\sigma(x)$ is defined as the exponential of the squared Mahalanobis distance to the unit:

$$\sigma(x) = \exp(\tilde{d}^2(x)),$$

where $\tilde{d}^2(x)$ is the squared Mahalanobis distance, and x is an evaluated point.

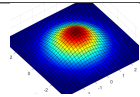
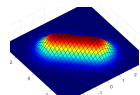
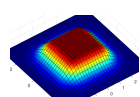
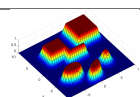
III. METHODOLOGY

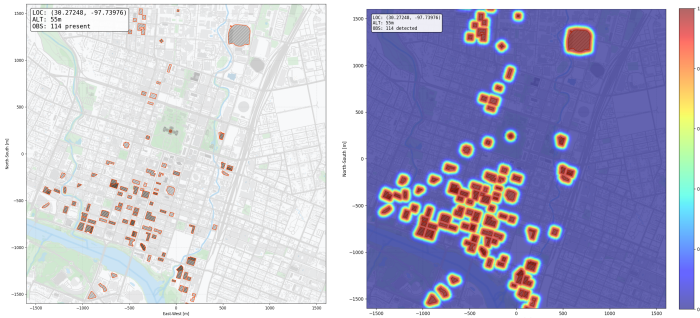
Leveraging the properties of the standardized risk field defined in Section II-B, we introduce *Larp Path Planner* (Last-mile Autonomous Route Planning Path Planner), a framework designed for risk-aware urban air mobility. The core of this framework is a multi-scale decomposition algorithm that partitions an urban environment into distinct risk-aware sectors. These sectors form the foundation for a low-altitude routing graph that prioritizes risk minimization. Fig. 2 demonstrates this decomposition applied to Austin, TX, USA, for an operating altitude of 50–60 meters AGL within a 1.6 km radius.

A. Multi-Scale Risk-Aware Cell Decomposition

Drawing inspiration from adaptive quad tree structures, the primary phase of our method involves partitioning the risk field into a hierarchy of cells. Each cell is assigned a discrete “Risk Zone” representing the maximum potential for restriction violation within its bounds. The subdivision strategy is adaptive: cells proximal to obstacles are refined to a higher granularity (smaller size), while open airspace is represented by larger cells. This approach significantly reduces the search space while augmenting routing precision near hazards. The decomposition process is detailed in Algorithms 1 and 2.

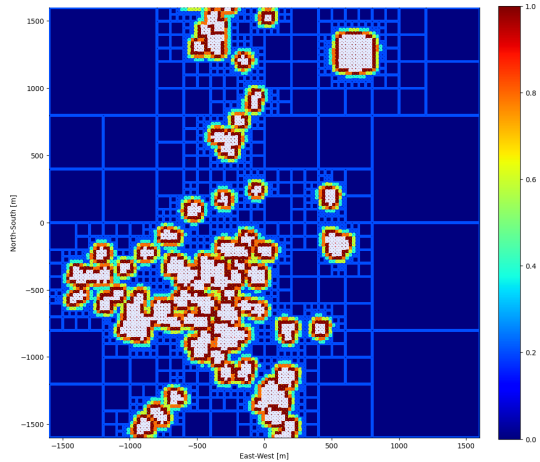
I. Risk Field Unit Definitions and Repulsion Vector Formulations.

Unit	Parameters	Repulsion vector $\bar{x}(x)$	Field
Point	Location \hat{x} Repulsion matrix A	$\bar{x}_p(x) = x - \hat{x}$	
Line	Line start \hat{x}_1 Line end \hat{x}_2 Repulsion matrix A	$\rho(x) = \frac{(\hat{x}_2 - \hat{x}_1) \cdot (x - \hat{x}_1)}{\ \hat{x}_2 - \hat{x}_1\ ^2}$ $\bar{x}_l(x) = x - \hat{x}_1 + \text{clamp}(\rho(x), 0, 1)(\hat{x}_2 - \hat{x}_1)$	
Polygon	Vertices $V = \{\hat{x}_1, \dots, \hat{x}_n\}$ Repulsion matrix A	$\bar{v}_i(x) = \text{Line}_{\bar{v}_i}(x, \hat{x}_i, \hat{x}_{i+1})$ $k = \text{argmin}_i \ \bar{v}_i(x)\ _A$ $\bar{x}_{po}(x) = \begin{cases} 0 & x \in \mathcal{P} \\ \bar{v}_k(x) & \text{otherwise} \end{cases}$	
Collection	Parameters of the sub units	<i>Repulsion vector $\bar{x}(x)$ of sub unit with smallest Mahalanobis distance $\hat{d}(x)$</i>	



(a) Austin, TX, USA

(b) Corresponding Risk Field



(c) Risk-Aware Multi-Scale Cell Decomposition

Fig. 2: Risk-aware multi-scale cell decomposition of Austin, TX (50–60m AGL). White cells mark obstacle zones; color denotes risk level.

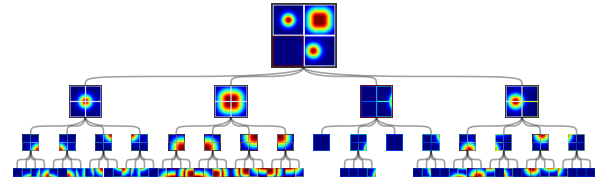


Fig. 3: Quad tree subdivision of a simple risk field. Cells refine recursively until risk falls below the safety threshold or minimum resolution is reached.

1) *Quad Tree Structure Construction*: Algorithm 1 outlines the recursive subdivision of the field. The process begins by initializing a root node representing the entire map. For each quadrant, the maximum risk is estimated via Algorithm 2. Based on this estimate, a decision is made to either classify the node as a leaf or subdivide it further.

Subdivision continues until one of two stopping criteria is met: 1) the cell is classified as the safest (lowest risk) zone, or 2) the cell reaches the minimum defined size limit (n_{min}). To optimize performance, obstacles located far outside the influence range of a specific quadrant are pruned from the set U during recursive calls. The leaves of the resulting tree constitute the multi-scale discretization of the allowable airspace. An example of the quad tree structure is presented in Fig. 3 for a simple field.

2) *Risk Estimation and Zone Assignment*: The heart of the decomposition efficiency is the ability to analytically estimate the risk upper bound of a cell without exhaustive sampling. This is achieved via Algorithm 2.

First, we calculate the squared Euclidean distance from the cell center to each obstacle. If this distance is less than the cell's circumscribed radius, the cell potentially contains the obstacle and is immediately assigned to Zone 0 (Obstacle Zone).

Algorithm 1 Larp Path Planner - Adaptive Cell Decomposition

```

1: function BUILD( $x, n, U$ )
2:    $quad \leftarrow QuadNode(x, n)$ 
3:    $zones \leftarrow$  map with default farthest zone
4:   if  $|U| > 0$  then
5:      $zones \leftarrow APPROXOBSTACLESZONES(x, n, U)$ 
6:   end if
7:    $quad.zone \leftarrow \min(zones)$   $\triangleright$  Assign conservative risk
8:   if  $n \leq n_{max}$  then
9:     if  $n \leq n_{min}$  or  $quad.zone$  is safest zone then
10:      Mark  $quad$  as leaf
11:      return  $quad$ 
12:    end if
13:  end if
14:   $U \leftarrow \{u \in U \mid zones[u] < safest\ zone\}$ 
15:  for each quad  $q$  of a cell do
16:     $quad.child[q] \leftarrow BUILD(q.center, n/2, U)$ 
17:  end for
18:  return  $quad$ 
19: end function
20:  $root \leftarrow BUILD(field.center, field.size, all\ units)$ 

```

Algorithm 2 Larp Path Planner – Zone Risk Estimation

Require: Sorted list of boundaries bds in descending order

```

1: function APPROXOBSTACLESZONES( $x, n, U$ )
2:    $zones \leftarrow$  default safe zone map
3:   for each unit  $u$  in  $U$  do
4:     if  $d_u^2(x) \leq \frac{n^2}{2}$  then
5:        $zones[u] \leftarrow 0$   $\triangleright$  Obstacle inside cell
6:     end if
7:   end for
8:   for each unit  $u$  in  $U$  not in  $zones$  do
9:      $c \leftarrow x - \frac{n}{\sqrt{2} \|\bar{x}_u(x)\|} \bar{x}_u(x)$   $\triangleright$  Project to edge
10:     $p \leftarrow \exp(-d_u^2(c))$ 
11:     $zones[u] \leftarrow Bin(p, bds)$ 
12:  end for
13:  return  $zones$ 
14: end function

```

For obstacles outside the cell boundary, we utilize the Mahalanobis distance. Using the obstacle’s repulsion vector, we project a point c on the circumscribed circle boundary closest to the obstacle. The risk $\sigma(c)$ is evaluated at this point. The maximum risk contribution from any obstacle determines the cell’s final Zone assignment. This guarantees that the assigned Zone represents a conservative upper bound of the risk within that cell.

Fig. 4 illustrates this approximation. The repulsion vectors are projected from the center to the extent of the cell’s diagonal. The magnitude of the vector and the risk at the boundary inform the maximum possible risk $\sigma_{max} \approx 0.8$ for that region, allowing for rapid classification without dense grid sampling.

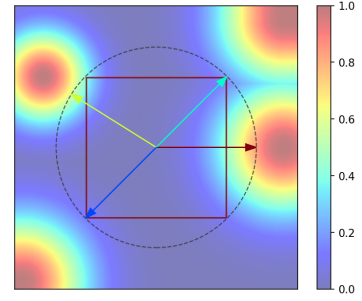


Fig. 4: Conservative risk upper bound estimation for a cell. Risk is evaluated at the intersection of the cell’s circumscribed circle and the obstacle’s repulsion vector.

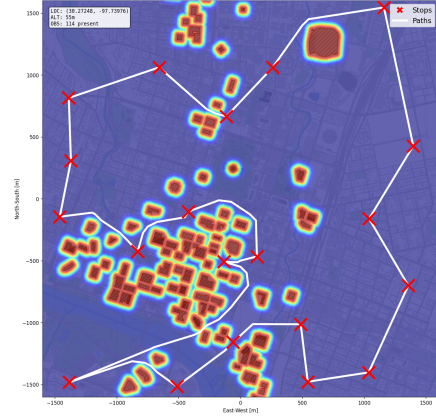


Fig. 5: Aggregated delivery routes over Austin, TX (55m AGL), demonstrating efficient traversal of open areas and dense downtown corridors.

B. Risk-Aware Global Planning

1) *Network Graph Construction:* Following decomposition, a connectivity graph is constructed. A divide-and-conquer strategy traverses the quad tree to identify adjacency relationships between leaf nodes. This transforms the continuous risk field into a discrete weighted graph where nodes represent risk-aware sectors and edges represent feasible transitions.

2) *Path Search:* To generate optimal routes, we employ a modified A* algorithm. The standard Euclidean distance cost function is augmented to penalize high-risk traversals:

$$d(q_a, q_b) = s(q_b) \cdot \|q_a.center - q_b.center\| \quad (1)$$

where q_a and q_b denote the current and target quadrants, respectively, and $s(q_b) \geq 1.0$ is a scaling factor derived from the Risk Zone of q_b . This effectively dilates the distance of high-risk edges, guiding the solver toward safer corridors unless a significant shortcut justifies the increased risk.

Once a sequence of nodes is identified, the path is smoothed using line-of-sight optimization to produce flight-ready waypoints. Fig. 5 depicts the resulting aggregated delivery routes for the Austin simulation.

IV. EXPERIMENTS AND RESULTS

A. Experimental Setup

The simulations utilized real-world urban data extracted via OpenStreetMap (OSM) for five distinct urban environments, chosen to represent varying degrees of obstacle density complexity. The search space for each environment was defined by a specific operating altitude and a radial extent ranging from 1.0 km to 2.5 km:

- 1) **Austin, TX (Downtown) & Boston, MA (Seaport):** Mid-rise urban layouts with irregular boundaries (Altitude: 50m; Radius: 1.6 km).
- 2) **Singapore (Marina Bay & Lucky Plaza):** A mixture of open water bodies and ultra-dense commercial corridors (Altitude: 50–70m; Radius: 1.0–2.0 km).
- 3) **Hong Kong (Central):** An environment characterized by extreme verticality and "urban canyons" (Altitude: 150m; Radius: 2.5 km).

We benchmark our *Adaptive Larp Path Planner* against three baselines: 1) **M-APF** [14], [20], a local reactive planner with anisotropic repulsion; 2) **Informed RRT*** [9], [10], a sampling-based asymptotically optimal planner (averaged over multiple stochastic trials); and 3) **Larp Path Planner (Fixed Grid)**, an ablation study using a uniform grid decomposition to isolate the benefits of the multi-scale approach.

Performance metrics include Success Rate (percentage of collision-free paths), Compute Time, Peak Risk (maximum risk encountered), Cumulative Risk (path integral of risk), and Path Length.

B. Comparative Analysis

Table II summarizes the aggregate performance across 750+ path planning queries.

1) *Success Rate and Efficiency:* The proposed Multi-Scale Larp Path Planner achieved a 100% success rate across all tested environments. In contrast, local reactive methods (M-APF) suffered in dense environments like Lucky Plaza and Hong Kong, frequently becoming trapped in local minima (73.5% success rate).

In terms of computational cost, our method demonstrated order-of-magnitude improvements over sampling-based approaches. While Informed RRT* required an average of 6.42 ± 6.97 seconds to converge to a solution, Larp Path Planner (Adaptive) generated paths in 0.01 ± 0.01 seconds. This rapid computation is critical for enabling real-time replanning in dynamic UAM operations.

2) *Risk Minimization:* A key contribution of this work is the explicit minimization of risk. As shown in Table II, Larp Path Planner yielded the lowest Cumulative Risk (12.04). While Informed RRT* produces short paths, it often "clips" corners of high-risk zones to optimize for Euclidean distance, resulting in significantly higher cumulative risk (38.43) and peak risk (0.24). Our method balances path length with risk avoidance, resulting in slightly longer paths (approx. 7% increase over RRT*) that are significantly safer.



(a) Boston, MA

(b) Generated Routes.

Fig. 6: Risk field and planned routes for Boston, MA. Safe regions (dark blue) are preferred; high-risk zones (dark red) are avoided.

C. Scalability: Fixed Grid vs. Multi-Scale Decomposition

To isolate the benefits of the multi-scale approach, we compared our Adaptive method against a Fixed Grid implementation of the same risk field (Table II, Rows 3 vs 4).

The Multi-Scale approach reduced computation time by approximately 85% compared to the Fixed Grid (0.01s vs 0.07s). In large open areas (e.g., over the water in Marina Bay or above parks in Austin), the adaptive quad-tree consolidates space into fewer, larger nodes, drastically reducing the search space for the A* planner. Conversely, in dense clusters, the grid refines automatically to capture narrow corridors. The Fixed Grid approach, forced to maintain high resolution everywhere to ensure safety in narrow passages, suffers from combinatorial explosion in the graph size. This comparison highlights the criticality of multi-scale decomposition for achieving city-scale scalability.

D. Qualitative Results in Dense Urban Sectors

Fig. 5 and 6 illustrate the generated paths for Boston and Austin, respectively. The risk-aware nature of the planner is evident in the trajectory behavior: the UAV maintains a high clearance from obstacles in open space (minimizing risk) but is capable of traversing narrow "urban canyons" when necessary to reach a destination.

In extremely dense scenarios (Fig. 7), the planner successfully navigates the crevices formed by building clusters. The risk field creates a cost topology that guides the planner through the centerline of avenues, treating the proximity of building surfaces as soft constraints that are only approached when no topological alternative exists.

V. CONCLUSION

Safe and scalable path planning is a prerequisite for low-altitude UAM, yet existing methods fail to simultaneously satisfy computational, safety, and city-scale demands. The Larp framework addresses this through risk-aware multi-scale cell decomposition, enabling verifiably safe global path planning

II. Quantitative Performance Comparison Across 750+ Path Planning Trials in Five Urban Environments.

Algorithm	Success Rate	Compute Time [s]	Peak Risk [σ]	Cumul. Risk [σ]	Path Length [m]
M-APF	73.5%	0.21 ± 0.28	0.04 ± 0.07	13.56 ± 32.87	701.99 ± 431.12
Informed RRT*	79.0%	6.42 ± 6.97	0.24 ± 0.32	38.43 ± 59.52	717.71 ± 415.24
Larp Path Planner (Fixed Grid)	100.0%	0.07 ± 0.10	0.10 ± 0.15	16.66 ± 29.65	749.21 ± 511.35
Larp Path Planner (Adaptive)	100.0%	0.01 ± 0.01	0.08 ± 0.14	12.04 ± 24.14	769.72 ± 530.45

[^] Metrics computed only on successful trials.

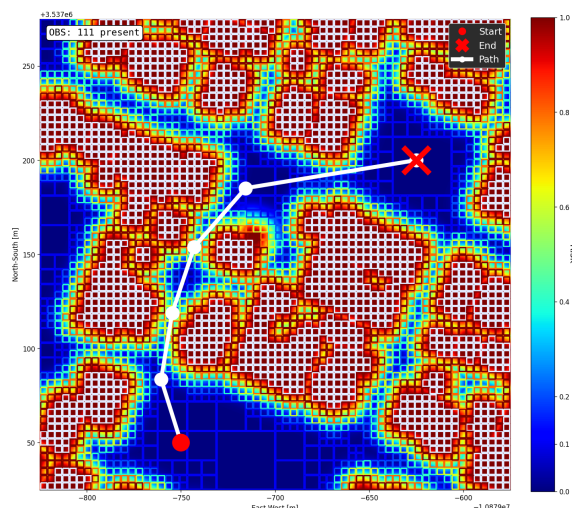


Fig. 7: Close-up of Larp Path Planner navigating a dense urban cluster, identifying safe corridors through the building infrastructure.

from any GeoJSON map input. Across 750+ trials in five urban environments, the adaptive planner achieved a 100% success rate, the lowest cumulative risk of any evaluated method (12.04, a 69% reduction over Informed RRT* (38.43)), and near-real-time computation (0.01 ± 0.01 s, over $600\times$ faster than Informed RRT* and 85% faster than the fixed-grid ablation), with only a $\sim 7\%$ path length overhead, confirming that multi-scale decomposition is critical for city-scale scalability.

Future work will pursue tighter risk bounding to reclaim usable airspace in highly restrictive sectors, and extending the static quadtree into a dynamic structure for real-time updates, enabling the framework to adapt to moving obstacles and evolving flight restrictions within an active UAM and UTM ecosystem. The source code is publicly available at <https://github.com/wzjoriv/Larp>.

REFERENCES

- [1] Y. Li, T. Guo, J. Chen, J. Wu, Y. Zhang, S. Alam, K. Cai, and W. Du, "Urban air mobility: A review and challenges," *IEEE Intelligent Transportation Systems Magazine*, vol. 17, no. 3, pp. 67–87, 2024.
- [2] A. Bauranov and J. Rakas, "Designing airspace for urban air mobility: A review of concepts and approaches," *Progress in Aerospace Sciences*, vol. 125, p. 100726, 2021.
- [3] B. Sah, R. Gupta, and D. Bani-Hani, "Analysis of barriers to implement drone logistics," *International Journal of Logistics Research and Applications*, vol. 24, no. 6, pp. 531–550, 2021.

- [4] R. Shrestha, I. Oh, and S. Kim, "A survey on operation concept, advancements, and challenging issues of urban air traffic management," *Frontiers in Future Transportation*, vol. 2, p. 1, 2021.
- [5] K. Telli, O. Kraa, Y. Himeur, A. Ouamane, M. Boumechraz, S. Atalla, and W. Mansoor, "A comprehensive review of recent research trends on unmanned aerial vehicles (uavs)," *Systems*, vol. 11, no. 8, p. 400, 2023.
- [6] C. Charnsethikul, J. M. Silva, W. J. C. Verhagen, and R. Das, "Urban air mobility aircraft operations in urban environments: A review of potential safety risks," *Aerospace*, vol. 12, no. 4, p. 306, 2025.
- [7] S. Ghambari, M. Golabi, L. Jourdan, J. Lepagnet, and L. Idoumghar, "UAV path planning techniques: A survey," *RAIRO-Operations Research*, vol. 58, no. 4, pp. 2951–2989, 2024.
- [8] H. Mazaheri, S. Goli, and A. Nourollah, "A survey of 3D space path-planning methods and algorithms," *ACM Computing Surveys*, vol. 57, no. 1, pp. 1–32, 2024.
- [9] J. D. Gammell, S. S. Srinivasa, and T. D. Barfoot, "Informed rrt*: Optimal sampling-based path planning focused via direct sampling of an admissible ellipsoidal heuristic," in *2014 IEEE/RSJ international conference on intelligent robots and systems*. IEEE, 2014, pp. 2997–3004.
- [10] —, "Batch informed trees (bit*): Sampling-based optimal planning via the heuristically guided search of implicit random geometric graphs," in *2015 IEEE international conference on robotics and automation (ICRA)*. IEEE, 2015, pp. 3067–3074.
- [11] J. Chen, M. Li, Z. Yuan, and Q. Gu, "An improved a* algorithm for uav path planning problems," in *2020 IEEE 4th Information Technology, Networking, Electronic and Automation Control Conference (ITNEC)*, vol. 1. IEEE, 2020, pp. 958–962.
- [12] C. Ju, Q. Luo, and X. Yan, "Path planning using an improved a-star algorithm," in *2020 11th International Conference on Prognostics and System Health Management (PHM-2020 Jinan)*. IEEE, 2020, pp. 23–26.
- [13] Y. K. Hwang and N. Ahuja, "A potential field approach to path planning," *IEEE transactions on robotics and automation*, vol. 8, no. 1, pp. 23–32, 1992.
- [14] S. M. H. Rostami, A. K. Sangaiah, J. Wang, and X. Liu, "Obstacle avoidance of mobile robots using modified artificial potential field algorithm," *EURASIP Journal on Wireless Communications and Networking*, vol. 2019, no. 1, pp. 1–19, 2019.
- [15] X. Fan, Y. Guo, H. Liu, B. Wei, and W. Lyu, "Improved artificial potential field method applied for auv path planning," *Mathematical Problems in Engineering*, vol. 2020, no. 1, p. 6523158, 2020.
- [16] Z. Wang, S. X. Ng, and E.-H. Mohammed, "Deep reinforcement learning assisted uav path planning relying on cumulative reward mode and region segmentation," *IEEE Open Journal of Vehicular Technology*, vol. 5, pp. 737–751, 2024.
- [17] B. Pang, X. Hu, W. Dai, and K. H. Low, "Uav path optimization with an integrated cost assessment model considering third-party risks in metropolitan environments," *Reliability Engineering & System Safety*, vol. 222, p. 108399, 2022.
- [18] A. Pilko, A. Söbester, J. P. Scanlan, and M. Ferraro, "Spatiotemporal ground risk mapping for uncrewed aircraft systems operations," *Journal of Aerospace Information Systems*, vol. 20, no. 3, pp. 126–139, 2023.
- [19] J. N. Rivera and D. Sun, "Air traffic management for collaborative routing of unmanned aerial vehicles via potential fields," in *2024 International Conference on Research in Air Transportation (ICRAT)*, 2024.
- [20] F. Bounini, D. Gingras, H. Pollart, and D. Gruyer, "Modified artificial potential field method for online path planning applications," in *2017 IEEE Intelligent Vehicles Symposium (IV)*. IEEE, 2017, pp. 180–185.